

Electronic structure of CdTe nanocrystals: A tight-binding study

Jesús Pérez-Conde

Departamento de Física, Universidad Pública de Navarra, E-31006 Pamplona, Spain

A. K. Bhattacharjee

Laboratoire de Physique des Solides, URA au CNRS, Université Paris-Sud, 91405 Orsay, France

(August 1, 2018)

We present a symmetry-based calculation of the electronic structure of a compound semiconductor quantum dot (QD) in the sp^3s^* tight-binding model including the spin-orbit interaction. The Hamiltonian matrix is diagonalized exactly for CdTe QD sizes up to 60 Å. The surface dangling bonds are passivated by hydrogen through a careful analysis of the density of states and wave functions. The calculated size dependence of the energy gap shows a reasonable agreement with the available experimental data. Our symmetry analysis indicates that, in contrast with a reported prediction of the three-band effective-mass model, the fundamental interband transition remains dipole-allowed in CdTe nanocrystals.

PACS Numbers: 73.20.Dx, 71.24.+q, 71.15.Fv, 78.40.Fy

I. INTRODUCTION

Semiconductor nanocrystallites, also called quantum dots (QD's), have been studied in recent years.¹ In particular, high-quality crystallites of II-VI compounds have been fabricated and their optical properties investigated in detail.^{2,3} The confinement-induced blueshift of the fundamental gap and the discretization of the energy spectrum have been observed. Early theoretical studies^{4,5} were based on the effective mass approximation (EMA), which was progressively refined by taking into account the degeneracy of the valence band.⁶⁻⁹ Generally speaking, the EMA overestimates the confinement energy in small QD's. Lippens and Lannoo¹⁰ reported a tight-binding (TB) calculation of the QD energy gap based on the empirical sp^3s^* model, previously developed by Vogl *et al.*¹¹ for bulk semiconductors. They used the recursion method and obtained a better agreement with experimental data than the EMA calculations. Nair *et al.*¹³ presented a different TB approach based on an effective-bond-orbital model.¹⁴ The pseudopotential method has also been successfully applied to some QD's.^{16,17}

Ren and Dow¹⁸ developed an algorithm for exact diagonalization of the TB Hamiltonian for a hydrogenated Si cluster in the sp^3s^* model by using the tetrahedral (T_d) symmetry. More recently, Albe *et al.*¹⁹ reported TB calculations for ZnS and CdSe QD's, also based on an exact diagonalization of the cluster Hamiltonian, but *including* the spin-orbit interaction. However, the “brute force” method, suitable for studying the QD shape effects they focused on, is rather limited to small sizes and does not allow any symmetry analysis of the QD eigenstates.

In this paper we report a symmetry-based TB study of the electronic structure of a zincblende semiconductor crystallite of roughly spherical shape in the sp^3s^* model including the spin-orbit interaction. Thus, our approach generalizes that of Ref. 18 to binary compounds and a

finite spin-orbit interaction. Here we apply it to CdTe, because substantial experimental data^{3,20,21} are available and a thorough three-band EMA study⁹ has been reported, allowing a detailed comparison with our results.

The paper is organized as follows. We first present an outline of the model in Section II, including the method of passivation of the surface states through hydrogen bonding. We present and discuss some results for CdTe QD's in Section III. The size dependence of the energy and the symmetry classification of a few conduction and valence band edge states are shown. The variation of the energy gap is compared with the available experimental data and the results of other published calculations. Finally, an analysis of the orbital symmetry of the highest valence band and the lowest conduction band states is carried out in order to check the electric dipole selection rule for the fundamental transition. The paper closes with some concluding remarks.

II. THE MODEL

The spin-independent part of the TB Hamiltonian is given by,^{11,12}

$$H_0 = \sum_{b, \mathbf{R}_b, i, \sigma} |\mathbf{R}_b, i, \sigma\rangle E_{i,b} \langle \mathbf{R}_b, i, \sigma| + \sum_{\langle \mathbf{R}_a, \mathbf{R}_c \rangle, i, j, \sigma} |\mathbf{R}_a, i, \sigma\rangle V_{i,j} \langle \mathbf{R}_c, j, \sigma| + \text{H.c.}, \quad (1)$$

where $b = a$ (anion), c (cation). \mathbf{R}_b are the atomic position vectors. i and j denote the orthonormal atomic orbitals s, p_x, p_y, p_z and s^* , which depend on b . σ is the z component of spin (\uparrow and \downarrow). Note that s^* represents an excited s state introduced phenomenologically in order to obtain a correct description of the conduction band in bulk semiconductors. The interatomic matrix elements $V_{i,j}$ are restricted to the nearest neighbors as indicated by $\langle \mathbf{R}_a, \mathbf{R}_c \rangle$ in the summation index. 13 independent parameters then characterize H_0 for a compound semiconductor, which are chosen to fit the known band structure. For example, the parameters for CdTe are given by¹² $E_{s,a} = -8.891$, $E_{p,a} = 0.915$, $E_{s,c} = -0.589$, $E_{p,c} = 4.315$, $V_{s,s} = -4.779$, $V_{x,x} = 2.355$, $V_{x,y} = 4.124$, $V_{s,p} = 1.739$, $V_{p,s} = -4.767$, $E_{s^*,a} = 7.0$, $E_{s^*,c} = 7.5$, $V_{s^*,p} = 1.949$, $V_{p,s^*} = -2.649$ eV. The spin-orbit coupling part of the Hamiltonian mixes the spin-up and spin-down p orbitals on the same atom:

$$H_{\text{SO}} = \sum_{b, \mathbf{R}_b, \sigma, \sigma', i, j} |\mathbf{R}_b, i, \sigma\rangle 2\lambda_b \mathbf{L}_b \cdot \mathbf{S}_b \langle \mathbf{R}_b, j, \sigma'|. \quad (2)$$

It introduces 2 additional parameters. $\lambda_a = 0.367$ and $\lambda_c = 0.013$ eV for CdTe.¹² When H_{SO} is included a more convenient atomic basis is given by the spin-orbit coupled orbitals, which are basically the total angular momentum eigenstates $|\mathbf{R}_b, j, j_z\rangle$ ($j = 3/2, 1/2$) that diagonalize the spin-orbit interaction. We, however, write them in terms

of the basis functions $|\mathbf{R}_b, u_m^k\rangle$ of the irreducible representations Γ_k ($k = 6, 7, 8$) of the tetrahedral point group T_d with respect to the site \mathbf{R}_b . Note that we have two sets of Γ_6 orbitals at a given site arising from the s and s^* states. Using the phase convention and coupling coefficients of Ref. 15, the first rows are

$$\begin{aligned} |u_{-1/2}^6(s)\rangle &= |s\rangle|\downarrow\rangle, \\ |u_{-1/2}^7(p)\rangle &= -\frac{i}{\sqrt{3}}|p_x\rangle|\uparrow\rangle - \frac{1}{\sqrt{3}}|p_y\rangle|\uparrow\rangle + \frac{i}{\sqrt{3}}|p_z\rangle|\downarrow\rangle, \\ |u_{-3/2}^8(p)\rangle &= -\frac{i}{\sqrt{6}}|p_x\rangle|\downarrow\rangle + \frac{1}{\sqrt{6}}|p_y\rangle|\downarrow\rangle + \frac{i\sqrt{2}}{\sqrt{3}}|p_z\rangle|\uparrow\rangle. \end{aligned}$$

Let us now construct a cluster of roughly spherical shape starting from, say, a cation at the origin by successively adding nearest-neighbor atoms through tetrahedral bonding. The dangling bonds emanating from the atoms generated in the last step will be passivated by placing a hydrogen s orbital at each empty nearest-neighbor site. This “hydrogenated” crystallite has an overall tetrahedral symmetry. We can, therefore, reduce the Hamiltonian to a block diagonal form by rewriting it in a symmetrized basis corresponding to the double-valued representations Γ_k ($k = 6, 7, 8$) of T_d .

Following the procedure developed in Ref. 14, we first construct the symmetrized site functions ϕ_n^i , corresponding to the single-valued representations Γ_i ($i = 1, 2, 3, 4, 5$) of T_d . All atoms at a given distance R_b from the origin constitute a shell. The sites $\{\mathbf{R}_b\}$ on a given shell are grouped into (generally more than one) symmetry subshells, each containing all sites which transform into one another under the 24 symmetry operations of T_d with respect to the QD center. Each subshell $\{\mathbf{R}\}$ is then spanned by the functions ϕ_n^i which represent symmetrized linear combinations of sites, assuming the values $\phi_n^i(\mathbf{R})$ at \mathbf{R} . These values are deduced by using the projection operators. Note that, except for the one-dimensional representations Γ_1 and Γ_2 , an irreducible representation generally occurs more than once in a given subshell. The site functions are then coupled with the localized atomic orbitals and the subshell basis functions of total symmetry Γ_k ($k = 6, 7, 8$) obtained as linear combinations of $\sum_{\mathbf{R}} \phi_n^i(\mathbf{R})|\mathbf{R}, u_m^j\rangle$, by using the coupling coefficients for Γ_k in $\Gamma_i \times \Gamma_j$.

The hydrogen shells are treated in a similar way. Here we have only one s -orbital per atom so that the local basis is restricted to the Γ_6 symmetry: $|\mathbf{R}_H, u_m^6\rangle$. Finally, in the symmetrized basis, the total Hamiltonian becomes block diagonal, each block corresponding to a given symmetry Γ_i ($i = 6, 7, 8$). This implies a substantial reduction of the size of the matrix to diagonalize. For example, for a cluster containing 3109 semiconductor atoms plus 852 H, instead of a matrix of size $32794 = 10 \times 3109 + 2 \times 852$ we get two equivalent Γ_6 matrices of size 2740, two equivalent Γ_7 matrices of size 2739 and four equivalent Γ_8 matrices of size 5459. Thus, the matrix size has been reduced by a factor of 6.

While the TB parameters enumerated above are assumed to be the same as those for the bulk semiconductor, we need to precise the parameters concerning the hy-

drogen atoms. The H energy level is obtained through the same scaling prescription as that for the cation and anion s levels.¹² In the case of CdTe, we obtain $E_{s,H} = -5$ eV. The hopping matrix elements between the anion or cation and H are assumed to follow the Harrison scaling rule: $V_{b-H} = (d_{a-c}/d_{b-H})^2 V_{ac}$, in terms of the bond lengths. d_{b-H} are usually¹⁸ taken from molecular data. In the absence of such data on Cd-H or Te-H bonds, we estimate the bond lengths by summing the corresponding covalent radii. This procedure typically yields the experimental bond lengths to within a few hundredths of angstrom. We thus obtain $d_{\text{Cd-H}} = 1.71$ and $d_{\text{Te-H}} = 1.67$ Å. The above parametrization scheme is adequate for passivating the surface dangling bonds in Si and Ge nanocrystals.¹⁸ However, in the case of CdTe, as shown in the next section, it is necessary to readjust (reduce) the bond lengths in order to completely eliminate the surface states from the electronic spectrum in the neighborhood of the forbidden gap.

III. RESULTS AND DISCUSSION

Let us first discuss the saturation of dangling bonds, as we are basically dealing with surface-passivated QD systems which show a systematic increase of the optical energy gap with decreasing size. The electronic density of states (DOS) as well as its hydrogen projected part, as calculated from the exact eigenstates of the TB Hamiltonian, are partly shown in Fig. 1 for a CdTe QD of diameter $D = 58.67$ Å containing $N = 3109$ semiconductor atoms. Note that $D \equiv a(3N/4\pi)^{1/3}$. The uppermost spectrum (a) corresponds to the CdTe cluster without H. Notice the large number of states in the bulk band gap region between 0 and 1.6 eV, which arise from the surface dangling bonds. Next we show the results (b) for the hydrogenated cluster (852 H atoms) with the standard bond length parameters: $d_{\text{Cd-H}} = 1.71$ and $d_{\text{Te-H}} = 1.67$ Å. Most of the surface states have disappeared, but not all. In fact, as seen from the hydrogenic partial DOS superposed on the total DOS, the lowest unoccupied (conduction) states are still surface states. We have directly verified this through the spatial distribution of the wave function. This is in contrast with the cases of Si or Ge where a complete saturation of dangling bonds is achieved by using the molecular bond lengths for the couplings with H atoms. As shown in Fig. 1 (c), in order to eliminate surface states from the relevant part of the electronic spectrum in our CdTe QD, we need to increase the couplings with H. By choosing bond lengths slightly shorter than before, $d_{\text{Cd-H}} = 1.58$ and $d_{\text{Te-H}} = 1.54$ Å, the hydrogenic DOS in the conduction band vanishes up to ~ 2 eV. We have checked that the same set of bond length parameters assures surface passivation in all the QD's considered.

Now we present the energies and wave functions of CdTe quantum dots of several sizes (see Table I). We

have chosen cation- and anion-terminated crystallites alternatingly in order to show the typical oscillating behavior of energy levels in the clusters of binary compounds.¹⁹ For instance, two crystallites of similar diameters, 12.35 and 13.15 Å, and terminated by cation and anion shells, respectively, present the lowest unoccupied state (LUS) at 2.11 and 2.42 eV. This is in contrast with the monotonous decrease observed in Si or Ge crystallites. The valence states also show such oscillations but with a smaller amplitude. In general, the LUS energy of a cation-terminated crystallite is higher than that of an anion-terminated crystallite of neighboring size, because of the dominating contribution from the cation s orbital to the conduction band. In Figures 2 and 3 we plot a few energy levels below and above the bandgap, respectively, against the QD size. The symmetry classification of the levels is also indicated. Note that for all sizes the LUS (conduction band) is of Γ_6 symmetry and the highest occupied state (HOS) of the valence band belongs to Γ_8 , as in the bulk semiconductor. For comparison, we include the respective energies calculated in the EMA (Ref. 9) which are shown as the solid curves. As usual, the EMA confinement energies are much larger than the TB ones in small-size QD's. However, the HOS (Fig. 2) shows a better convergence with increasing size, which reminds us that the TB model yields a better description of the valence band in the bulk semiconductor.

The calculated QD bandgap E_g , the energy difference between the LUS and HOS, is plotted as a function of size in Fig. 4. We also present a compilation of the available experimental values of the optical bandgap. The results of previous EMA (Ref. 9) and TB (Ref. 10) calculations are also shown. In contrast with these calculations, however, we have not corrected E_g for the electron-hole Coulomb interaction. Thus, the closeness of our results to those of Lippens and Lannoo¹⁰ shown as the dashed curve is rather misleading. Their uncorrected gap would be systematically larger than ours; this is probably related to the neglect of spin-orbit coupling in their calculation. It can be seen that the size dependence of our uncorrected E_g shows a good qualitative agreement with experiment. The calculated values are somewhat smaller, but they are simply based on the parameters of Ref. 12 for bulk CdTe, which we prefer not to modify in any arbitrary manner. There is also some uncertainty related to the parameters concerning the H atoms. As for the Coulomb correction, it is rather difficult to evaluate consistently within the TB model. But we expect it to be significantly smaller than that estimated from the EMA used in the calculations cited above, because the TB carrier wave functions are spatially more extended (see Fig. 5).

Figure 5 shows the shell-wise radial distribution of the carrier probability density for the LUS (electron) and HOS (hole) states in a QD of diameter 58.67 Å. The shell probability density for an eigenstate $|\Psi\rangle$ is directly obtained from the diagonalization of the TB Hamiltonian, by summing the local density $P(\mathbf{R}_b) \equiv \sum_{i,\sigma} | \langle$

$\mathbf{R}_b, i, \sigma |\Psi\rangle^2$ over the sites \mathbf{R}_b on the given shell. We see that, in contrast with the smooth EMA envelope functions, the TB radial distributions are oscillatory. It is interesting to note that the LUS (HOS) is indeed preponderant at the cation (anion) shells. In the present case the cation (anion) shells account for 79% (76%) of the LUS (HOS). Another reason for the oscillatory behavior is the discontinuous variation of the number of atoms on a shell. All the oscillations are, of course, smoothed over in the EMA. It is not easy to make a direct comparison. However, it can be verified that our TB charge distributions have a greater radial extension than the EMA envelope functions.

Finally, in order to reexamine the electric-dipole selection rules for the fundamental interband transition, we present an analysis of the orbital symmetry of the full wave functions in the TB model. We proceed as follows. By setting the spin-orbit interaction $H_{\text{SO}} = 0$, we first diagonalize H_0 in the spin-degenerate atomic orbital basis. The resulting eigenvalues are then classified according to the single-valued representations Γ_i ($i = 1 - 5$). As the second step, we diagonalize the same Hamiltonian in the spin-orbit coupled basis: the same eigenvalues are now classified in terms of the double-valued representations Γ_i ($i = 6 - 8$), which arise from the direct products of Γ_6 with Γ_i ($i = 1 - 5$). By consulting the multiplication table of the group T_d , we see that there are three different types of Γ_8 corresponding to the three orbital symmetries Γ_3 , Γ_4 and Γ_5 . Thus, the eigenstates Γ_8^0 of H_0 can be identified as $\Gamma_8^0(\Gamma_3)$, $\Gamma_8^0(\Gamma_4)$ or $\Gamma_8^0(\Gamma_5)$. Finally, a given eigenstate Γ_8 of the full Hamiltonian, for example the HOS, can be written as a linear combination of all the ‘unperturbed’ states $\Gamma_8^0(\Gamma_i)$ ($i = 3 - 5$). By calculating the projections and summing the probabilities over all states arising from a given orbital symmetry Γ_i , we can deduce the fractional contribution of that symmetry in the HOS. Similarly, an eigenstate Γ_6 such as the LUS can be analyzed in terms of the orbital symmetries Γ_1 and Γ_4 .

The numerical results for the CdTe QD’s are as follows. The LUS is found to be almost pure Γ_1 for all sizes: 99.9% for $D = 12.35 \text{ \AA}$ and 99.7% for $D = 58.67 \text{ \AA}$. The results for the HOS (Γ_8) are more interesting; they are shown in Table II. Note that our numerical calculation was limited to the contributions from the nine topmost ‘unperturbed’ valence states for each of the single-valued representations, because of the huge size of the data files involved. This is, however, adequate for identifying the majority component in all cases. We find that the Γ_3 contribution is always small. On the other hand, as the QD size increases the *dominant* orbital symmetry of the HOS changes from Γ_4 to Γ_5 . Thus, for $D \geq 17.8 \text{ \AA}$ the fundamental interband transition is certainly dipole-allowed. In Fig. 2 we notice that the second highest valence state is also of Γ_8 symmetry and lies very close to the HOS. We, therefore, analyzed its orbital symmetry as well; the results are presented inside parentheses in Table II. It is interesting to observe that its dominant orbital sym-

metry also changes with increasing size, but from Γ_5 to Γ_4 , in a manner opposite to the HOS. Anyway, the QD size where this second level approaches the HOS is large enough so that no further ‘symmetry cross-over’ is expected, because the HOS in the bulk is indeed Γ_5 -like. To sum up, the fundamental transition is *almost* dipole-forbidden for $D \leq 13.2 \text{ \AA}$, but certainly dipole-allowed for $D \geq 17.8 \text{ \AA}$. Clearly, our results contradict the prediction of Lefevre *et al.*⁹. They found that in the three-band EMA the HOS (hole ground state) in a CdTe QD, regardless of the size, has a *p*-type envelope function, making it dipole-forbidden for optical transitions with the *s*-type LUS. Let us point out that although our analysis is inadequate for calculating the actual transition probabilities, it does allow an unambiguous identification of the symmetry forbidden transitions.

IV. CONCLUDING REMARKS

We have presented a TB calculation of the electronic structure of a roughly spherical semiconductor QD of tetrahedral symmetry. It is based on the sp^3s^* empirical TB model¹¹ that accounts for the band structure of bulk semiconductors. The use of group theory allows not only a substantial reduction in size of the Hamiltonian matrix to diagonalize, but also a symmetry analysis of the eigenstates. Our treatment represents a generalization of the previous work by Ren and Dow¹⁸ to binary compounds and a finite spin-orbit interaction. Here we have applied the model to the case of CdTe. Through a careful analysis of the DOS spectrum we have explicitly passivated the surface dangling-bond states. The calculated one-electron bandgap as a function of size shows a reasonable agreement with the available experimental values of the optical bandgap. We find that, regardless of the QD size, the valence band HOS and the conduction band LUS belong to Γ_8 and Γ_6 symmetries, respectively, as in the bulk semiconductor. However, an analysis of the orbital symmetry reveals that, while the LUS is almost pure Γ_1 -like for all sizes, the *dominant* orbital symmetry of the HOS changes from Γ_4 for $D \leq 13.2 \text{ \AA}$ to Γ_5 for $D \geq 17.8 \text{ \AA}$. Thus, except for very small QD’s, the electric dipole transitions remain allowed between the HOS and the LUS, in contradiction with the three-band EMA result reported previously.

ACKNOWLEDGMENTS

This work was supported in part by the spanish DGI-CyT under contract no. PB95-0797.

- ¹ For a review see Y. Wang and N. Herron, J. Phys. Chem. **95**, 525 (1991).
- ² D. J. Norris and M. G. Bawendi, Phys. Rev. B **53**, 16 338 (1996).
- ³ Y. Masumoto and K. Sonobe, Phys. Rev. B **56**, 9734 (1997).
- ⁴ Al. L. Efros and A. L. Efros, Sov. Phys. Semicond. **16**, 772 (1982).
- ⁵ Y. Kayanuma, Solid State Commun. **59**, 405 (1986); Phys. Rev. B **38**, 9797 (1988); Y. Kayanuma and H. Momiji, Phys. Rev. B **41**, 10261 (1990).
- ⁶ J.-B. Xia, Phys. Rev. B **40**, 8500 (1989).
- ⁷ G. B. Grigoryan, E. M. Kazaryan, Al. L. Efros, and T. V. Yazeva, Sov. Phys. Solid State **32**, 1031 (1990).
- ⁸ P. C. Sercel and K. J. Vahala, Phys. Rev. B **42**, 3690 (1990).
- ⁹ P. Lefevre, T. Richard, H. Mathieu, and J. Allègre, Solid State Commun. **98**, 303 (1996); T. Richard, P. Lefevre, H. Mathieu, and J. Allègre, Phys. Rev. B **53**, 7287 (1996).
- ¹⁰ P. E. Lippens and M. Lannoo, Phys. Rev. B **39**, 10 935 (1989); Semicond. Sci. Technol. **6**, A157 (1991).
- ¹¹ P. Vogl, H. P. Hjalmarson, and J. D. Dow, J. Phys. Chem. Solids **44**, 365 (1983).
- ¹² A. Kobayashi, O. F. Sankey, and J. D. Dow, Phys. Rev. B **25**, 6367 (1982).
- ¹³ S. V. Nair, L. M. Ramaniah, and K. C. Rustagi, Phys. Rev. B **45**, 5969 (1992).
- ¹⁴ G. T. Einevoll and Y.-C. Chang, Phys. Rev. B, **40**, 9683 (1989).
- ¹⁵ G. F. Koster, J. O. Dimmock, R. G. Wheeler and H. Statz, *Properties of the Thirty-Two Point Groups (MIT Press, Cambridge, MA, 1963)*.
- ¹⁶ M. V. Rama Krishna and R. A. Friesner, Phys. Rev. Lett. **67**, 629 (1991).
- ¹⁷ L. W. Wang and A. Zunger, Phys. Rev. Lett. **73**, 1039 (1994).
- ¹⁸ S. Y. Ren and J. D. Dow, Phys. Rev. B **45**, 6492 (1992); S. Y. Ren, Phys. Rev. B **55**, 4665 (1997).
- ¹⁹ V. Albe, C. Jouanin, and D. Bertho, J. Crystal Growth **184/185**, 388 (1998); Phys. Rev. B **58**, 4713 (1998).
- ²⁰ T. Rajh, O. I. Micic, and A. J. Nozik, J. Phys. Chem. **97**, 11999 (1993).
- ²¹ Y. Mastai and G. Hodes, J. Phys. Chem. B **101**, 2685 (1997).

D (Å)	N	N_H	Last shell	$E(\text{HOS})$	$E(\text{LUS})$
10.34	17	36	cation	-1.101	2.909
12.35	29	36	anion	-1.083	2.113
13.15	35	36	cation	-0.969	2.427
17.81	87	76	anion	-0.719	1.951
24.95	239	196	cation	-0.393	2.059
32.43	525	276	anion	-0.303	1.721
43.08	1231	460	cation	-0.177	1.775
58.67	3109	852	cation	-0.104	1.696

TABLE I. Some important features of the QD's analyzed. The first column gives the diameter. The second and third columns give the numbers of semiconductor and hydrogen atoms, respectively. The fourth column specifies the atom type of the terminating shell. The last two columns show the calculated HOS and LUS energies in eV.

D (Å)	Γ_3	Γ_4	Γ_5
12.35	3.88(6.85)	84.15(17.07)	11.57(75.92)
13.15	4.87(4.48)	90.26(33.84)	3.78(49.03)
17.81	4.25(0.54)	22.04(80.10)	68.74(18.16)
24.95	0.10(0.20)	0.11(87.84)	96.54(1.26)
32.43	1.43(0.60)	33.27(63.65)	54.57(31.30)
43.08	1.81(0.99)	26.35(67.71)	58.81(26.43)
58.67	1.68(0.77)	26.91(65.44)	56.70(27.58)

TABLE II. Size dependence of the percentage contributions of different orbital symmetries in the HOS. Inside parentheses we show the corresponding values for the nearest state in energy (also Γ_8), which is almost degenerate for $D > 30$ Å.

FIG. 1. Total density of states (dashed curve) and its hydrogenic part (solid curve) for $D = 58.67$ Å: (a) No passivation, (b) H passivation with the bond lengths $d_{\text{Te-H}} = 1.67$ and $d_{\text{Cd-H}} = 1.71$ Å, (c) H passivation with the bond lengths $d_{\text{Te-H}} = 1.54$ and $d_{\text{Cd-H}} = 1.58$ Å

FIG. 2. Energies and symmetries of the ten highest occupied (valence band) levels *versus* the QD diameter. The solid curve shows the three-band EMA result from Ref. 9 for the highest level.

FIG. 3. Energies and symmetries of the ten lowest unoccupied (conduction) levels *versus* the QD diameter. The solid curve is the EMA result for the lowest level.

FIG. 4. Size dependence of the energy gap: Results of the present calculation are shown as open triangles connected by solid lines. Experimental data for the optical gap are from Refs. 20 (open diamonds), 21 (filled squares), and 3 (open circles). Previous calculations in the TB model (Ref. 10) and the EMA (Ref. 9) are shown as the dashed and dotted curves, respectively.

FIG. 5. Shell-wise radial distribution of the carrier probability density in the HOS (a) and LUS (b) for $D = 58.67$ Å.

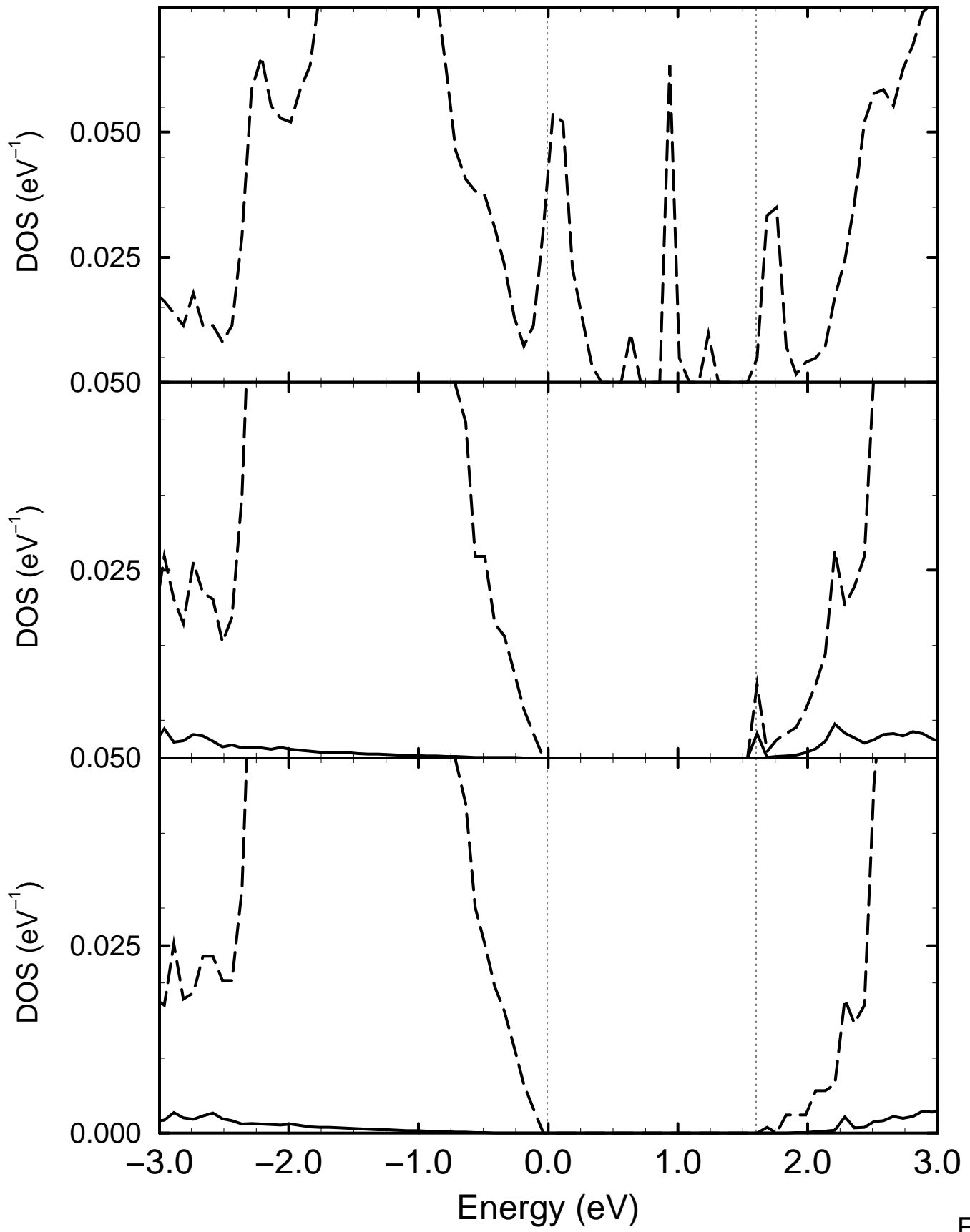


Fig.1

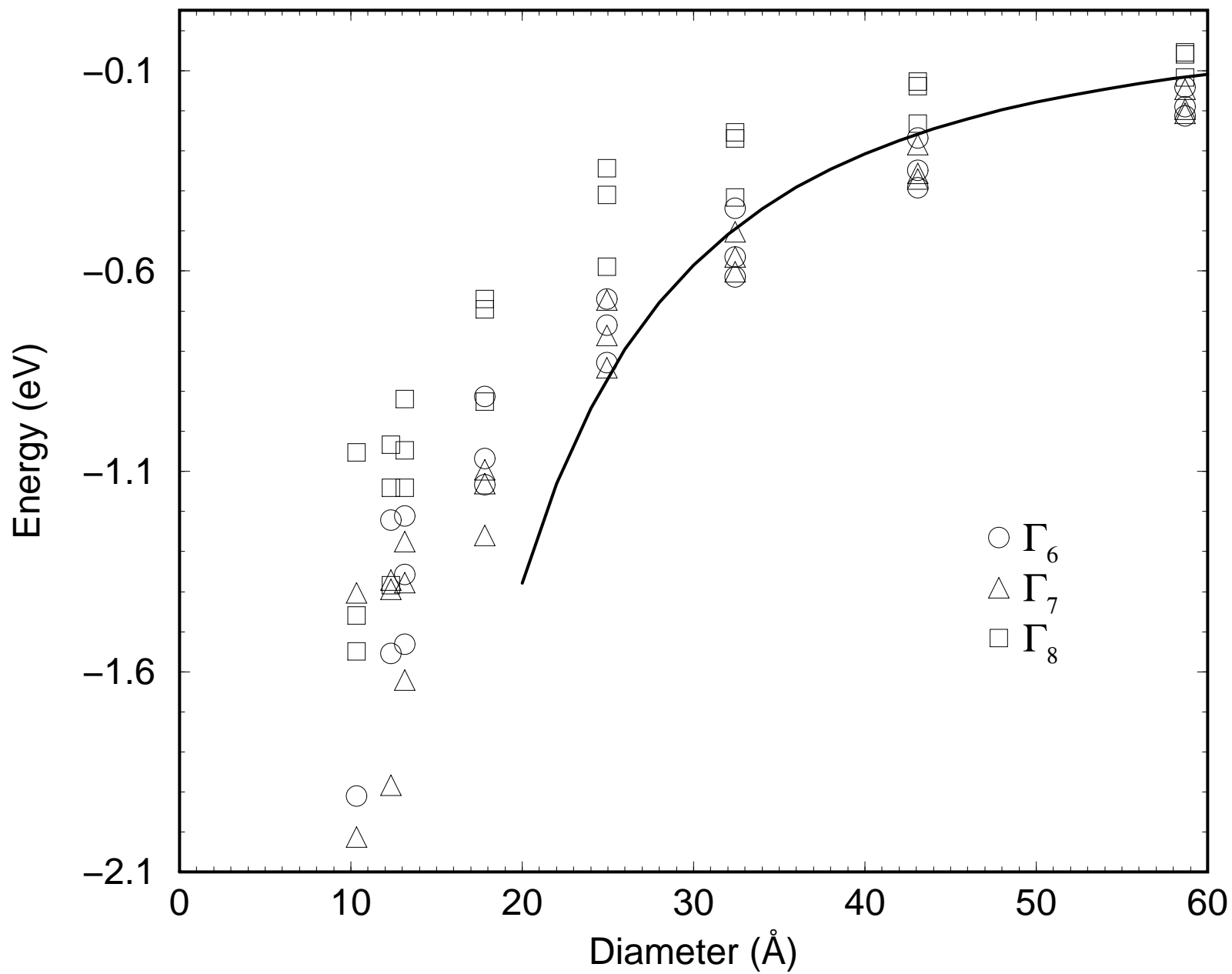


Fig.2

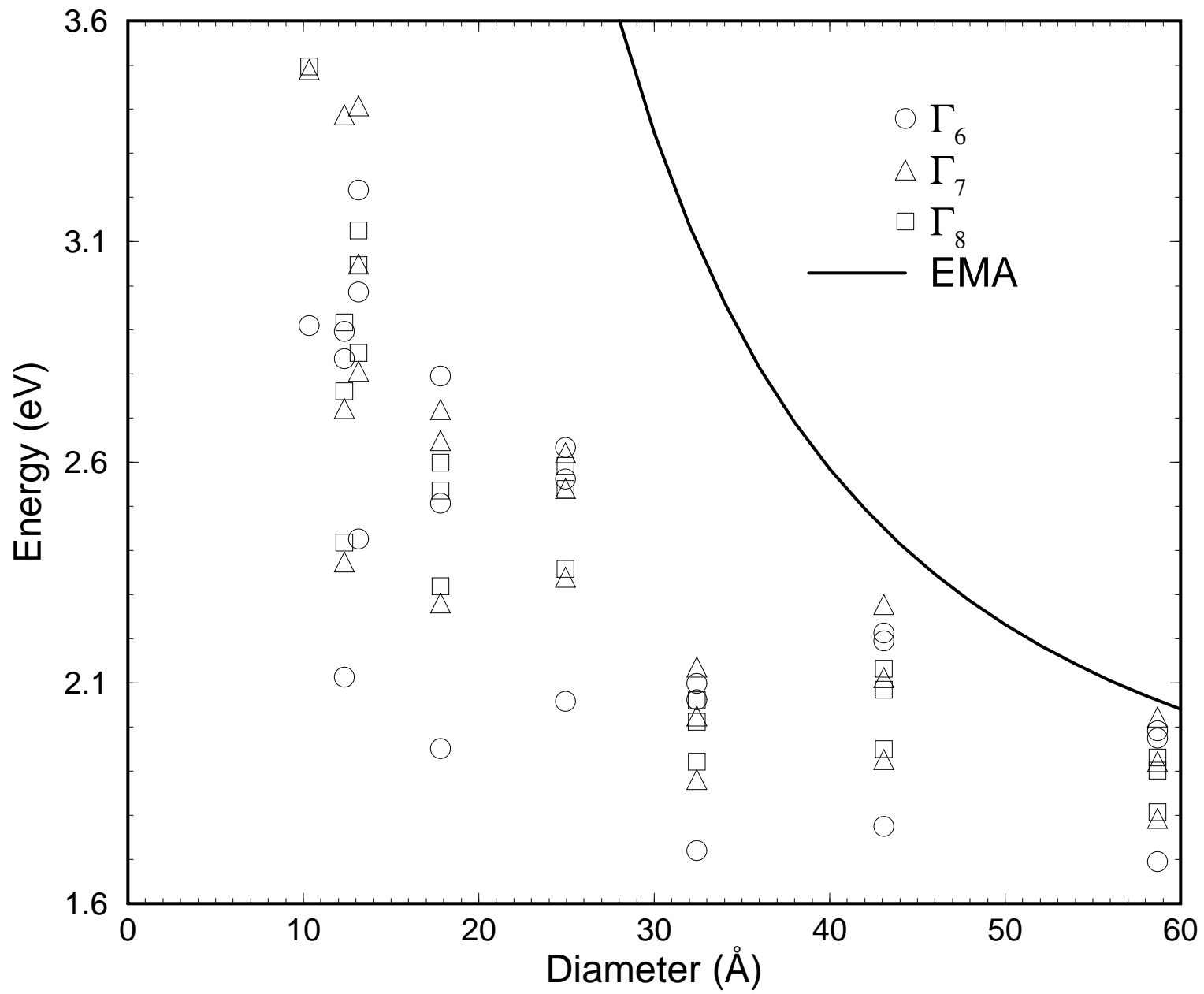


Fig. 3

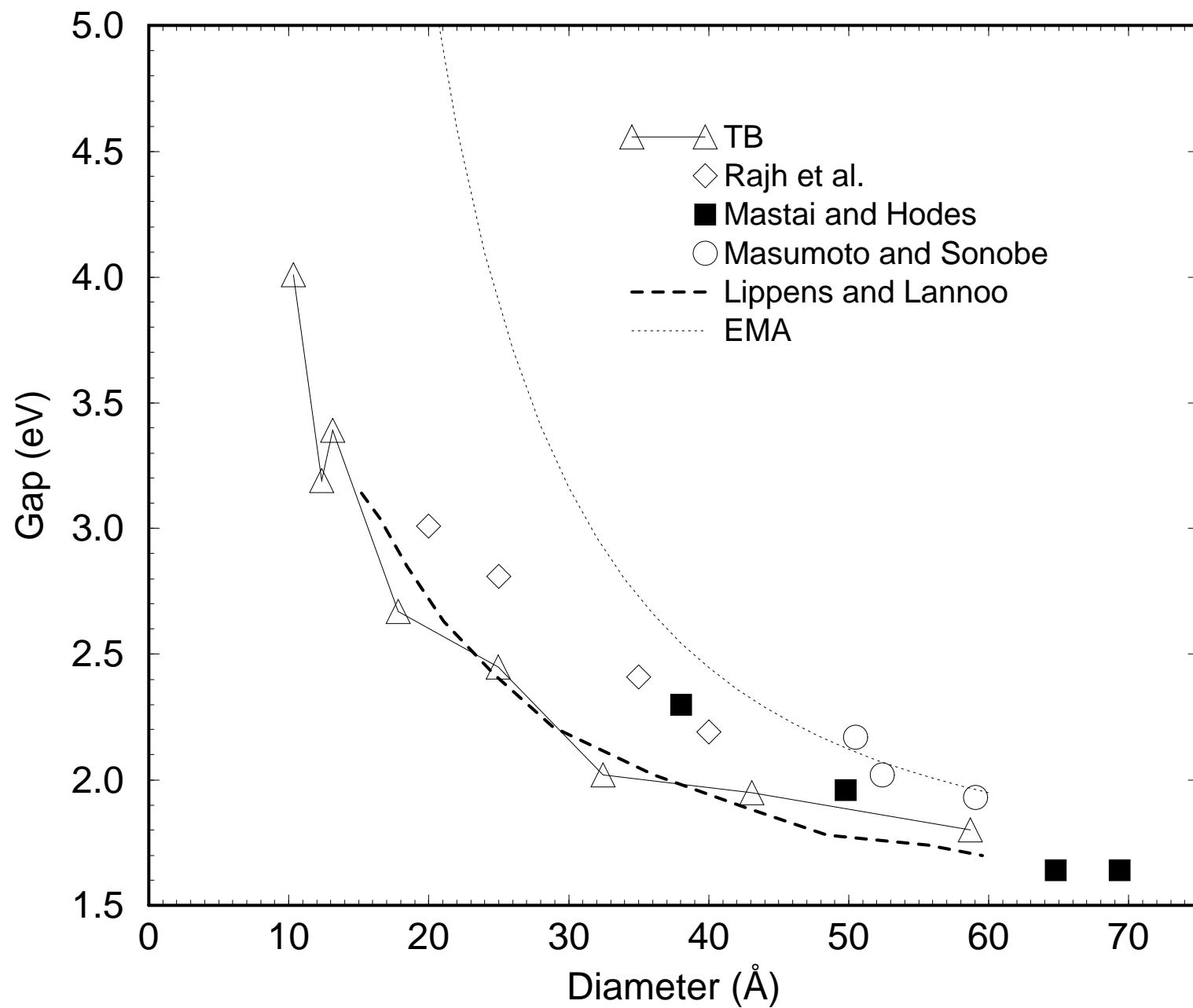


Fig.4

